# Revisiting Gaussian Process Reconstruction for Cosmological Inference: The Generalised GP (Gen GP) Framework

 $Ruchika, ^{1,2,3}$  Purba Mukherjee, <sup>4</sup> and Arianna Favale<sup>5,6</sup>

<sup>1</sup> Departamento de Física Fundamental and IUFFyM, Universidad de Salamanca, E-37008 Salamanca, Spain

<sup>2</sup> INFN, Sezione di Roma, Piazzale Aldo Moro 2, I-00185 Roma, Italy

<sup>3</sup> Directionental di Física Università di Roma "La Sezionea", Piazzale Aldo Moro 2, I-00185 Roma (L. 100185 Roma (L. 100185 Roma), Italy

<sup>3</sup> Dipartimento di Fisica, Università di Roma "La Sapienza", Piazzale Aldo Moro 2, I-00185 Roma, Italy
<sup>4</sup> Centre for Theoretical Physics, Jamia Millia Islamia, New Delhi-110025, India

#### ABSTRACT

We investigate uncertainties in the estimation of Hubble constant  $(H_0)$  arising from Gaussian Process (GP) reconstruction, demonstrating that the choice of kernel introduces systematic variations comparable to those arising from different cosmological models. To address this limitation, we introduce the Generalized Gaussian Process (Gen GP) framework, in which the Matérn smoothness parameter  $\nu$  is treated as a free parameter, allowing for data-driven kernel optimization. Using the cosmic chronometer Hubble data, we find that while standard GP with  $\Lambda$ CDM mean function exhibits noticeable reconstruction differences between optimized and marginalized approaches, particularly at z > 1, Gen GP maintains methodological consistency.

In Gen GP, slight increases in  $\chi^2$  per degree of freedom relative to standard GP, for both the zero-mean and  $\Lambda$ CDM prior mean cases, reflect added flexibility rather than performance degradation. Our results emphasize that robust cosmological inference requires treating kernel parameters as free variables and implementing full Bayesian marginalization to avoid artificial precision from fixed hyper-parameters. As machine learning becomes central to cosmological discovery, the Gen GP framework provides a principled approach to model-independent inference that properly accounts for methodological uncertainties while maintaining necessary flexibility for reliable parameter estimation.

Keywords: Cosmology, Gaussian Process Regression, Bayesian Marginalization, Hubble Parameter, Bias Correction, Statistical Methods

# 1. INTRODUCTION

Machine Learning has made a remarkable job in interpreting cosmological data in recent years C. Dvorkin et al. (2022); S. Ravanbakhsh et al. (2016). As we anticipate greater opportunities in the next decade, challenges also arise in adopting Machine Learning (hereafter ML) methodologies and extracting meaningful insights F. Villaescusa-Navarro et al. (2020). Its transformative potential lies in its ability to address cosmological issues such as identifying data clusters, handling sparse data and outliers, classifying datasets, and unraveling the physical intricacies within extensive datasets D. Baron (2019); I. Goodfellow et al. (2016). The versatility of ML holds promise for revolutionizing the field of cosmology, but a comprehensive understanding of challenges is crucial to harness its full potential for groundbreaking research in the coming years N. M. Ball & R. J. Brunner (2010); T. Charnock et al. (2020).

The applications of ML in cosmology are diverse and impactful. Notably, ML has demonstrated its ability to significantly reduce scatter in mass estimates of clusters compared to traditional methods M. Ntampaka et al. (2015); C. Modi et al. (2018). In the realm of weak lensing maps, where non-Gaussianities pose challenges in measurement and

Corresponding author: Ruchika Email: ruchika.science@usal.es

<sup>&</sup>lt;sup>5</sup> Dipartimento di Fisica, Università di Roma Tor Vergata, and INFN, Sezione di Roma 2, via della Ricerca Scientifica, 1, 00133, Roma, Italy

<sup>&</sup>lt;sup>6</sup>Departament de Física Quàntica i Astrofísica, Universitat de Barcelona, and Institut de Ciències del Cosmos, c. Martí i Franqués, 1, 08028 Barcelona, Catalonia, Spain

parameterization, ML emerges as a powerful solution J. Wilde et al. (2022); G.-J. Wang et al. (2022); J. Schmelzle et al. (2017); J. M. Zorrilla Matilla et al. (2020). Studies have demonstrated that these non-Gaussianities encode valuable cosmological information, leading to a remarkable tightening of parameter constraints by a factor of five or more D. Ribli et al. (2019); J. Merten et al. (2019). Additionally, for next-generation Cosmic Microwave Background (CMB) experiments, ML is shown to provide competitive methods for extracting a high signal-to-noise ratio of the projected gravitational potential from CMB sky maps J. Caldeira et al. (2019); G.-J. Wang et al. (2022); M. Münchmeyer & K. M. Smith (2019). ML's reach extends to predicting structure formation L. Lucie-Smith et al. (2024); J. Harnois-Dérap s et al. (2019) and classifying the earliest luminous sources that drove the reionization epoch S. Hassan et al. (2019). Furthermore, in photometric surveys like the Vera Rubin C. Observatory (LSST) R. Mandelbaum et al. (2018); Ž. Ivezić et al. (2019), ML is leveraged to classify supernovae, and this classification is subsequently utilized to obtain cosmological constraints M. Lochner et al. (2016). The myriad applications underscore ML's pivotal role in advancing our understanding of cosmological phenomena and shaping the future of observational cosmology.

While ML cannot replace statistical reasoning for well-modeled phenomena, the increasing precision in cosmological data enhances the theoretical gaps in the current understanding of the universe M. Raveri & W. Hu (2019); E. Sellentin & A. F. Heavens (2016). The standard model of cosmology, a spatially flat  $\Lambda$ -cold-dark-matter ( $\Lambda$ CDM) framework with nearly scale-invariant primordial power spectra, provides the best description of cosmological observations, including CMB anisotropies, large-scale structure (LSS) clustering, the magnitude-redshift relation of type Ia supernovae (SNIa), and weak lensing of both the CMB and LSS (cosmic shear) N. Aghanim et al. (2020); T. M. C. Abbott et al. (2022); C. Heymans et al. (2021). However, several observational hints raise fundamental questions, the most pronounced being the Hubble tension – now exceeding the  $5\sigma$  confidence level – between the Hubble constant  $H_0$  inferred from high-redshift CMB measurements ( $H_0 = 67.36 \pm 0.54$  km/s/Mpc) N. Aghanim et al. (2020) and that obtained from local SNIa observations ( $H_0 = 73.04 \pm 1.04$  km/s/Mpc) A. G. Riess et al. (2022); L. Verde et al. (2019); E. Di Valentino et al. (2021).

The existing state-of-the-art models (featuring both early and late time modifications to ΛCDM) struggle to explain all the cosmological datasets together L. Knox & M. Millea (2020); E. Mörtsell & S. Dhawan (2018); T. L. Smith et al. (2021); K. Dutta et al. (2020); Ruchika et al. (2023); A. I. Lonappan et al. (2018); J. Evslin et al. (2018); T. Patil et al. (2024); M. Forconi et al. (2023, 2024); C. Krishnan et al. (2020), paving the way for ML to play a vital role in the future of data-driven cosmological discovery. ML, however, poses a dual challenge: it accelerates discoveries in the face of upcoming data-intensive surveys A. Blanchard et al. (2020); R. Mandelbaum et al. (2018), yet tempts researchers to prioritize expediency over deep understanding, particularly in the presence of complex or rapidly increasing data volumes C. Dvorkin et al. (2022); N. Jeffrey et al. (2020). Acknowledging that small biases in ML are currently overshadowed by other systematics, it is imperative for the future to meticulously address and account for biases to ensure the robustness and accuracy of ML applications in the evolving landscape of cosmological research M. Ntampaka et al. (2019); T. Charnock et al. (2018); F. Villaescusa-Navarro et al. (2020).

Artificial Neural Networks A. Géron (2019); I. Goodfellow et al. (2016), Convolutional Neural Networks Y. LeCun et al. (2015), Gradient Boosting Regression J. H. Friedman (2001), Extra-Trees P. Geurts et al. (2006), Support Vector Machines C. Cortes & V. Vapnik (1995); K. P. Murphy (2012), Genetic Algorithms J. H. Holland (1992), and Gaussian Processes (GP) C. E. Rasmussen & C. K. I. Williams (2006); C. M. Bishop (2006) have emerged as powerful tools for deciphering intricate patterns within data, with GP notably finding applications in cosmological fields like parameter estimation M. Seikel et al. (2012); B. S. Haridasu et al. (2018); W. Handley (2019); M. Raveri & W. Hu (2019); Y. Yang & Y. Gong (2021); J. d. J. Velázquez et al. (2024); P. Mukherjee et al. (2024a), calibration of the distance ladders A. Gómez-Valent (2022); N. Liang et al. (2022); A. Favale et al. (2023); Z. Li et al. (2023); A. Favale et al. (2024); P. Mukherjee et al. (2024b, 2026), constraining CMB temperature evolution Ruchika et al. (2025), measuring the sound horizon at the drag epoch T. Lemos et al. (2023), and measuring Hubble constant A. Shafieloo et al. (2012); V. C. Busti et al. (2014); A. Gómez-Valent & L. Amendola (2018); Y. Yang et al. (2023).

In this work, we provide a detailed study of the Gaussian Process framework, incorporating the Cosmic Chronometers (CC hereafter) data (see, e.g., M. Moresco et al. (2022); M. Moresco (2024) for dedicated reviews). We introduced the Generalized Gaussian Process (Gen GP), an extension of traditional GP, that eliminates the inherent bias of the kernel. The results strongly emphasize the potential for continued progress in such cosmology-independent statistical techniques S. Ravanbakhsh et al. (2016); P. Berger & G. Stein (2019); S. Capozziello et al. (2019), reinforcing the assertion that data-driven inference frameworks are not only a promising future path but represent a dynamic field that requires ongoing refinement of methodologies to mitigate biases and ensure accurate training of cosmological

datasets E. Sellentin & A. F. Heavens (2016). We find that both the shapes of the Hubble function H(z) and its normalized definition,  $E(z) = H(z)/H_0$ , can be reconstructed with high accuracy when we keep the GP unbiased by choosing any particular kernel and cosmology-dependent prior mean function. While the impact of kernel and mean function choices has been discussed in previous literature (see, e.g. A. Shafieloo et al. (2012); T. Holsclaw et al. (2011, 2010); M. Seikel et al. (2012); A. Favale et al. (2023); S.-g. Hwang et al. (2023); J. P. Johnson & H. K. Jassal (2025); J.-y. Jiang et al. (2025); P. Mukherjee & A. A. Sen (2025, 2024); P. Mukherjee & N. Banerjee (2021)), here we take a deeper step by introducing a modification of the conventional GP framework. This allows us not only to assess these dependencies more rigorously but also to enhance the robustness of the reconstructed functions. Furthermore, we estimate cosmological parameters using the reconstructed H(z) and find that the results are consistent with those obtained directly from observational data.

This manuscript is organised as follows. Section 2 establishes the theoretical and methodological foundations essential for cosmological data interpretation through a dual approach. We first present the cosmological model landscape, examining various theoretical frameworks: the standard  $\Lambda$ CDM model, the constant equation of state wCDM, the dynamical Chevallier-Polarski-Linder (CPL) parametrization, and the cosmology model-independent Padé approximation. We then develop the statistical inference framework using Gaussian Processes, detailing the different kernel choices and prior mean functions, culminating in the introduction of our Generalized GP approach. This comprehensive treatment allows systematic analysis of how both theoretical model assumptions and statistical methodology choices fundamentally shape cosmological parameter inference. Section 3 presents the cosmological datasets and  $\chi^2$  minimization techniques employed in our analysis. Gaussian Process training method and the Prediction Algorithm is described in section 4. Section 5 present our results, discuss the implications for cosmological inference, and provide strong motivation for the Gen GP framework. Finally, Section 6 summarizes our conclusions and their broader implications for robust cosmological parameter estimation.

## 2. THE DUAL NATURE INFERENCE: COSMOLOGICAL MODELS AND STATISTICAL METHODS

## 2.1. Cosmological Framework

The flat ΛCDM model predicts the evolution of the normalized Hubble parameter with redshift as N. Aghanim et al. (2020); P. A. R. Ade et al. (2016):

$$\frac{H(z)}{H_0} = \left[\Omega_{m0}(1+z)^3 + (1-\Omega_{m0})\right]^{\frac{1}{2}},\tag{1}$$

where  $\Omega_{m0}$  represents the present-day matter density parameter and  $H_0$  is the Hubble constant.

The wCDM model introduces a constant equation of state parameter w for dark energy S. Weinberg (1989); T. Padmanabhan (2003), modifying the normalized Hubble parameter evolution to:

$$\frac{H(z)}{H_0} = \left[\Omega_{m0}(1+z)^3 + (1-\Omega_{m0})(1+z)^{3(1+w)}\right]^{\frac{1}{2}}.$$
 (2)

For enhanced flexibility in describing dark energy evolution, we employ the Chevallier-Polarski-Linder (CPL) parametrization M. Chevallier & D. Polarski (2001); E. V. Linder (2003). The CPL model incorporates a redshift-dependent equation of state parameter  $w(z) = w_0 + w_a(1-a) = w_0 + w_a\frac{z}{1+z}$ , where  $w_0$  and  $w_a$  characterize the present-day equation of state and its evolution, respectively. The corresponding normalized Hubble parameter is:

$$\frac{H(z)}{H_0} = \left[\Omega_{m0}(1+z)^3 + (1-\Omega_{m0})f(z)\right]^{\frac{1}{2}},\tag{3}$$

where  $f(z) = \exp \left[ 3 \int_0^z \frac{1+w(x)}{1+x} dx \right]$  M. Adachi & M. Kasai (2012).

We also investigate a Padé approximation approach for dark energy modeling A. Aviles et al. (2014), which avoids specific parametric assumptions about the dark energy equation of state. This method models deviations from a cosmological constant through a Taylor expansion of the dark energy density around the present epoch (z = 0):

$$\rho_{de}(a) = \rho_0 + \rho_1(1-a) + \rho_2(1-a)^2 + \dots$$
(4)

where  $\rho_0$ ,  $\rho_1$ , and  $\rho_2$  represent the present-day dark energy density and its first and second derivatives, respectively. Converting to redshift coordinates and applying a (2,2) Padé approximation C. Gruber & O. Luongo (2014), the

normalized Hubble parameter becomes:

$$\frac{H(z)}{H_0} = \left[\Omega_{m0}(1+z)^3 + (1-\Omega_{m0})\mathcal{P}(z)\right]^{\frac{1}{2}},\tag{5}$$

where

$$\mathcal{P}(z) = \frac{1 + P_1 z + P_2 z^2}{1 + Q_1 z + Q_2 z^2},\tag{6}$$

with  $P_1$ ,  $P_2$ ,  $Q_1$ , and  $Q_2$  serving as the four expansion parameters. This Padé parametrization encompasses a broad range of dark energy behaviors, including phantom-crossing scenarios and negative effective dark energy densities, while naturally reducing to  $\Lambda$ CDM in the limits of very low and very high redshifts.

## 2.2. Statistical Framework: Gaussian Processes

Gaussian Processes provide a non-parametric Bayesian approach for function reconstruction that has found extensive application in cosmological inference C. E. Rasmussen & C. K. I. Williams (2006). In cosmology, GP methods have been successfully employed to reconstruct the cosmic expansion history, matter distribution evolution, and structure growth from diverse observational datasets including SNIa, baryon acoustic oscillations (BAO), growth measurements, and CC (see, e.g, M. Seikel et al. (2012); A. Shafieloo et al. (2012); T. Holsclaw et al. (2011); B. S. Haridasu et al. (2018); P. Mukherjee & N. Banerjee (2021); P. Mukherjee & A. A. Sen (2024); A. Favale et al. (2023)).

The GP reconstruction framework depends critically on two fundamental components: the choice of kernel (covariance) function and the prior mean function D. J. C. MacKay (2002). These elements encode assumptions about the underlying physical process and substantially influence both the behavior and predictive capability of the GP reconstruction. Proper selection of these functions allows incorporation of physical knowledge while maintaining the flexibility necessary for reliable cosmological inference.

Given n observational data points  $y=(y_1,\ldots,y_n)$  at redshifts  $z=(z_1,\ldots,z_n)$  with covariance matrix C, the objective is to reconstruct the underlying function  $f^*=(f(z_1^*),\ldots,f(z_N^*))$  at new points  $z^*=(z_1^*,\ldots,z_N^*)$ , typically with N>n.

A Gaussian Process represents a generalization of the multivariate Gaussian distribution to function space, completely specified by a mean function  $\mu(z)$  and covariance function k(z, z') R. M. Neal (1996):

$$f \sim \mathcal{N}\left(\mu(z), k(z, z')\right)$$
 (7)

where  $k_{ij} = k(z_i, z_j)$  is defines the covariance matrix elements of covariance k(z, z').

## 2.2.1. Kernel Selection

The most commonly employed covariance function in cosmological applications is the squared exponential (SE) kernel T. Holsclaw et al. (2011):

$$k_{\rm SE}(r) = \sigma_f^2 \exp\left(-\frac{r^2}{l_f^2}\right) \tag{8}$$

where r = |z - z'|, and the hyperparameters  $\sigma_f$  and  $l_f$  control the signal variance and characteristic length scale, respectively M. Seikel et al. (2012).

Additionally, we consider the Double Squared Exponential (DSE) kernel, constructed as the sum of two SE kernels:

$$k_{\text{DSE}}(r) = \sigma_{f1}^2 \exp\left(-\frac{r^2}{l_{f1}^2}\right) + \sigma_{f2}^2 \exp\left(-\frac{r^2}{l_{f2}^2}\right),$$
 (9)

which increases modeling flexibility at the cost of doubling the number of hyperparameters.

For greater generality, one employs the Matérn class of covariance functions M. Seikel et al. (2012), which provides a more flexible framework for modeling correlation structures. The general Matérn kernel is defined as C. E. Rasmussen & H. Nickisch (2010):

$$k_{\nu}(r) = \sigma_f^2 \frac{2^{1-\nu}}{\Gamma(\nu)} \left(\frac{\sqrt{2\nu}r}{l_f}\right)^{\nu} K_{\nu} \left(\frac{\sqrt{2\nu}r}{l_f}\right), \tag{10}$$

where  $\Gamma$  is the gamma function,  $K_{\nu}$  is the modified Bessel function of the second kind M. Abramowitz & I. A. Stegun (1964), and  $\nu$  is a positive parameter controlling the smoothness of the process.

For half-integer values of  $\nu$ , the Matérn kernel simplifies to closed-form expressions T. Holsclaw et al. (2011); M. Seikel et al. (2012), viz.

$$k_{\nu=3/2}(r) = \sigma_f^2 \left( 1 + \frac{\sqrt{3}r}{l_f} \right) \exp\left( -\frac{\sqrt{3}r}{l_f} \right),$$

$$k_{\nu=5/2}(r) = \sigma_f^2 \left( 1 + \frac{\sqrt{5}r}{l_f} + \frac{5r^2}{3l_f^2} \right) \exp\left( -\frac{\sqrt{5}r}{l_f} \right),$$
and so on.

The parameter  $\nu$  determines the differentiability properties of the reconstructed function: processes with  $\nu=1/2$  are continuous but not differentiable, while larger values of  $\nu$  correspond to increasingly smooth functions. In the limit  $\nu \to \infty$ , the Matérn kernel converges to the squared exponential form R. M. Neal (1996). Previous studies suggest that  $\nu \le 7/2$  provides adequate flexibility for most cosmological applications C. E. Rasmussen & C. K. I. Williams (2006); A. Favale et al. (2023); N. Banerjee et al. (2023); P. Mukherjee & A. A. Sen (2024).

For enhanced generality and to avoid kernel selection bias, we employ the **Generalized Gaussian Process (Gen GP) framework**, which utilizes the Matérn class of covariance functions (see Equation 10). Unlike standard GP implementations that fix the smoothness parameter  $\nu$  to specific values, Gen GP treats  $\nu$  as a free parameter (with uniform prior  $\log_{10}(\nu) \in \mathcal{U}[-2,1]$  as detailed in Table 3), allowing the data to determine the optimal smoothness properties.

## 2.2.2. Prior Mean Function Selection

The prior mean function  $\mu(z)$  represents the initial assumption about the underlying function before observing data A. Shafieloo et al. (2012). This choice significantly impacts reconstruction quality, as an appropriate prior can reduce the dynamic range over which the GP must extrapolate from the data T. Holsclaw et al. (2011).

The most agnostic choice is the zero mean function,  $\mu(z) = 0$ , which avoids imposing specific cosmological assumptions. However, this approach may require large values of  $\sigma_f$  to accommodate the full range of observational data, potentially necessitating large correlation lengths  $l_f$  that could smooth away important features and compromise derivative reconstructions M. Seikel et al. (2012).

Alternatively, one can adopt a model-based prior mean function, such as the  $\Lambda$ CDM prediction. In this case, the GP models deviations from the assumed cosmological model as

$$\mu(z) = y_{\text{obs}} - y_{\Lambda \text{CDM}}(z), \qquad (12)$$

where  $y_{\Lambda \text{CDM}}(z)$  represents the theoretical prediction. While this approach can improve reconstruction efficiency, it introduces the risk that final results retain memory of the initial assumption, potentially biasing cosmological parameter estimates M. Seikel et al. (2012); A. Favale et al. (2023); S.-g. Hwang et al. (2023).

In our analysis, we examine both, a zero mean function for a more agnostic approach, and a  $\Lambda$ CDM-based mean function to assess the impact of theoretical priors on parameter inference L. Verde (2010). This comparative approach establishes a baseline that allows us to quantify the systematic effects of complex mean function choice on cosmological conclusions A. Shafieloo et al. (2012).

# 3. GP METHODOLOGY: HYPERPARAMETER SAMPLING AND LIKELIHOOD EVALUATION

This section focuses on generalising GP reconstruction to infer the Hubble function H(z) using CC measurements. These data have been collected over the past two decades via the differential age technique R. Jimenez & A. Loeb (2002), utilising massive and passively evolving galaxies observed up to redshift  $z \lesssim 2$  from different galaxy surveys.

Our analysis employs 32 cosmic chronometer measurements spanning redshifts  $0.07 \le z \le 1.965$ , compiled from multiple surveys mentioned in M. Moresco et al. (2022); M. Moresco (2024). These measurements, obtained via the differential age method applied to massive, passively evolving galaxies, provide direct constraints on H(z) independent of distance ladder calibrations or cosmological model assumptions. The full dataset is also available at Gitlab<sup>7</sup>.

<sup>7</sup> https://gitlab.com/mmoresco/CC\_covariance

# 3.1. Dataset Choice and Methodological Focus

Although a complete analysis would benefit from including multiple observational probes such as SNIa, BAO and CMB data, our work remains primarily methodological in nature. We aim to advance the GP framework for cosmological inference, addressing key issues such as hyperparameter uncertainties and kernel selection bias.

The deliberate choice to concentrate on CC data allows us to isolate and study the systematic effects inherent in GP reconstruction methods without the additional complexity introduced by combining heterogeneous datasets, each with its own systematic uncertainties and selection effects W. Sun et al. (2021). This allows us to isolate the methodological performance of different GP implementations in parameter inference and uncertainty quantification.

The extension to multi-probe cosmological analyses, while scientifically valuable, is beyond the scope of this work and represents a natural direction for future research. Once the methodological foundations established here are properly validated and understood, subsequent studies can apply these improved GP techniques to comprehensive datasets to obtain robust cosmological constraints. We plan to pursue such multi-dataset analyses in our future work, building upon the methodological framework developed in this paper.

# 3.2. Parameter Inference and Sampling Strategy

The core challenge in our approach is the efficient sampling of the GP hyperparameters, specifically  $\sigma_f$ ,  $l_f$ , and, in the Gen GP case, an additional parameter  $\nu$ . For restricted GP models using fixed values of  $\nu$  (e.g., Matérn kernels with  $\nu = 3/2$ , 5/2, 7/2, 9/2, or SE and DSE), the hyperparameter space consists of  $\{\sigma_f, l_f\}$  in addition to the standard cosmological parameters  $\Theta^*$ . In the Gen GP framework,  $\nu$  is treated as a free parameter, increasing the dimensionality of the parameter space to  $\Theta = \{\sigma_f, l_f, \nu\}$ .

Sampling these parameters in their natural units (linear-space) is inefficient due to their wide dynamic ranges and often complex posterior shapes. To overcome this, we adopt a logarithmic sampling approach, assigning flat priors in log-space, namely  $\log_{10}(\sigma_f)$ ,  $\log_{10}(l_f)$ , and  $\log_{10}(\nu)$ .

This transformation allows for more uniform exploration of parameter space and improves convergence. For  $\sigma_f$  and  $l_f$ , which can range from  $10^{-5}$  to  $10^{+5}$ , log-sampling ensures efficient coverage. For  $\nu$ , which typically ranges from  $10^{-2}$  (non-differentiable) to values above 1 (smooth functions), the log-scale avoids inefficient sampling near zero and improves numerical stability during matrix inversion.

Throughout the training process, sampling is performed entirely in log-space. When evaluating the likelihood and generating predictions, parameters are transformed back to their physical units:  $\sigma_f = 10^{\log_{10}(\sigma_f)}$ ,  $l_f = 10^{\log_{10}(l_f)}$ ,  $\nu = 10^{\log_{10}(\nu)}$ . This ensures the GP covariance matrix is constructed correctly while preserving the computational efficiency gained during sampling.

The Matérn kernel, which relies on the additional  $\nu$  to define smoothness, receives the back-transformed  $\nu$  value at each step, allowing the data to determine the appropriate level of differentiability. Posterior samples are also transformed back for final inference and uncertainty estimates.

Proper handling of these transformations is critical for avoiding biases and underestimation of uncertainties. The inclusion of  $\nu$  as a free parameter in the Gen GP framework is particularly important, as it allows the data to inform the optimal smoothness, thereby reducing the risk of kernel selection bias.

## 3.3. Bayesian Framework & Likelihood Evaluation

Parameter inference is carried out by maximising the GP log-marginal likelihood:

$$\ln \mathcal{L}(\Theta, \Theta^*) = -\frac{1}{2} \mathbf{y}^T K_y^{-1} \mathbf{y} - \frac{1}{2} \ln |K_y| - \frac{n}{2} \ln(2\pi), \tag{13}$$

where  $\mathbf{y} = \mathbf{H}_{\text{obs}} - \boldsymbol{\mu}(\mathbf{z})$  represents the residual vector between observations and the GP prior mean, and  $K_y = K(\mathbf{X}, \mathbf{X}^*) + C$  is the total covariance matrix, combining the kernel matrix K and the observational noise matrix C.

The first term in Eq. (13) quantifies the fit to the data, while the second term penalises overly complex models, functioning as an automatic Occam's razor. The final term ensures proper normalisation but does not affect parameter estimation directly.

To evaluate the inverse and determinant of  $K_y$ , we employ Cholesky decomposition, which guarantees numerical stability and computational efficiency across a wide range of hyperparameter values, including extreme or near-degenerate cases

The hyperparameters sampled in log-space are converted back to physical units at each likelihood evaluation step for the proposed parameter set  $\{\Theta, \Theta^*\}$  to ensure the GP covariance matrix is correctly constructed. This log-normal

likelihood structure forms the basis of our Bayesian framework and naturally incorporates both goodness-of-fit and model complexity.

## 3.3.1. Cosmological Model Analysis

For comparison with GP-based approaches, we also perform standard MCMC analysis for parametric cosmological models ( $\Lambda$ CDM, wCDM, CPL, Padé) using the same CC dataset. The likelihood is:

$$\mathcal{L}(\Theta^*) = \exp\left(-\frac{1}{2}\chi^2\right), \quad \chi^2 = [H_{\text{obs}} - H_{\text{model}}(z; \Theta^*)]^T C^{-1} [H_{\text{obs}} - H_{\text{model}}(z; \Theta^*)]$$
(14)

This provides model-dependent baselines for assessing GP reconstruction performance.

## 3.4. Implementation Details

We use the publicly available emcee<sup>8</sup> sampler D. Foreman-Mackey et al. (2013) to generate Markov Chain Monte Carlo chains, and analyse the resulting samples with GetDist<sup>9</sup> A. Lewis (2019). Our analysis pipeline also utilizes NumPy<sup>10</sup> C. R. Harris et al. (2020), SciPy<sup>11</sup> P. Virtanen et al. (2020), Astropy<sup>12</sup> T. P. Robitaille et al. (2013); A. M. Price-Whelan et al. (2018, 2022), and Matplotlib<sup>13</sup> J. D. Hunter (2007). For standard GP implementation, we use the GaPP<sup>14</sup> package M. Seikel et al. (2012) as a baseline for our analysis.

We adopt uniform priors over wide ranges for all parameters (as shown in Table 3), allowing the data to drive the inference without introducing strong prior assumptions. This is especially important for the GP hyperparameters, where restrictive priors can constrain the flexibility of the reconstruction and underestimate the associated uncertainties.

By allowing  $\nu$  to vary freely in the Gen GP case and sampling all GP hyperparameters in log-space, our approach provides a more flexible and unbiased framework for non-parametric cosmological inference.

| Kernel Type  | $H_0 \text{ (km/s/Mpc)}$ | $\sigma_{H_0} \; (\mathrm{km/s/Mpc})$ | $\sigma_{H_0}/H_0$ (%) | $\sigma_f$      | $l_f$        | $\chi^2/{ m dof}$ |
|--------------|--------------------------|---------------------------------------|------------------------|-----------------|--------------|-------------------|
| Matérn $3/2$ | 69.35                    | 6.34                                  | 9.13                   | 140.01          | 4.29         | 0.42              |
| Matérn $5/2$ | 69.28                    | 5.36                                  | 7.74                   | 132.54          | 2.90         | 0.45              |
| Matérn $7/2$ | 68.87                    | 5.08                                  | 7.37                   | 133.20          | 2.61         | 0.47              |
| Matérn $9/2$ | 68.50                    | 4.95                                  | 7.23                   | 135.57          | 2.54         | 0.48              |
| SE           | 67.18                    | 4.68                                  | 6.97                   | 148.81          | 2.53         | 0.49              |
| DSE          | 67.33                    | 6.39                                  | 9.49                   | [154.51, 10.08] | [3.19, 0.35] | 0.43              |

**Table 1.** Results at 68% C.L. on  $H_0$  with standard GP using different kernels and the values of their corresponding hyperparameters. Here, the a priori mean function is set to 0. The last column reports the values of  $\chi^2/\text{dof}$ , where the degrees of freedom (dof) are calculated as the number of data points minus fitted hyperparameters. See Sec. 5.1 for details.

| Model                  | $H_0 \text{ (km/s/Mpc)}$ | $\sigma_{H_0} \; ({\rm km/s/Mpc})$ | $\sigma_{H_0}/H_0$ (%) | $\chi^2/{ m dof}$ |
|------------------------|--------------------------|------------------------------------|------------------------|-------------------|
| $\Lambda \mathrm{CDM}$ | 68.84                    | 4.11                               | 5.97                   | 0.48              |
| wCDM                   | 70.11                    | 5.64                               | 8.05                   | 0.50              |
| CPL                    | 70.97                    | 6.04                               | 8.51                   | 0.51              |

**Table 2.** Comparison of  $H_0$  values across different cosmological models. See Sec. 5.1 for details.

## 4. GAUSSIAN PROCESS PREDICTION FRAMEWORK

Given a set of observed data  $\mathbf{y}$ , our goal is to estimate the function values  $\mathbf{f}^*$  at new test points  $\mathbf{X}^*$  where we need to calculate the predictions. The conditional distribution of  $\mathbf{f}^*$ , given the observed data and training inputs  $\mathbf{X}$ , follows

<sup>&</sup>lt;sup>8</sup> https://emcee.readthedocs.io/en/stable/

<sup>&</sup>lt;sup>9</sup> https://getdist.readthedocs.io/en/latest/

<sup>10</sup> https://numpy.org/

<sup>11</sup> https://scipy.org/

<sup>&</sup>lt;sup>12</sup> http://www.astropy.org

 $<sup>^{13}</sup>$  https://matplotlib.org

<sup>14</sup> https://github.com/carlosandrepaes/GaPP

a multivariate Gaussian:

$$\mathbf{f}^* \mid \mathbf{X}^*, \mathbf{X}, \mathbf{y} \sim \mathcal{N}\left(\overline{\mathbf{f}^*}, \operatorname{Cov}(\mathbf{f}^*)\right)$$
, (15)

with the predictive mean and covariance given by,

$$\overline{\mathbf{f}^*} = \mu^* + K(\mathbf{X}^*, \mathbf{X}) \left[ K(\mathbf{X}, \mathbf{X}) + C \right]^{-1} (\mathbf{y} - \mu), \tag{16}$$

and

$$Cov(\mathbf{f}^*) = K(\mathbf{X}^*, \mathbf{X}^*) - K(\mathbf{X}^*, \mathbf{X}) [K(\mathbf{X}, \mathbf{X}) + C]^{-1} K(\mathbf{X}, \mathbf{X}^*).$$
(17)

Here,  $K(\mathbf{X}, \mathbf{X})$  is the covariance matrix at the training inputs,  $K(\mathbf{X}^*, \mathbf{X})$  denotes the cross-covariance between test and training points, C accounts for the observational noise, and  $\mu$  and  $\mu^*$  are the prior mean functions evaluated at the training and test points, respectively. The predictive uncertainties at the test points are obtained from the diagonal of the covariance matrix  $Cov(\mathbf{f}^*)$ .

In practice, we implement this prediction using the following GaPP code wrapper function prediction

which returns the predicted mean and standard deviation. This function numerically allows us to evaluate the expression in Eq. (16), using provided training data  $z_{\rm CC}$ , test points  $z \equiv z_{\rm pred}$ , observational values  $H_{\rm CC} \equiv H(z_{\rm CC})$ , data covariance  $\Sigma_{\rm CC}$ , and the hyperparameters  $\{\Theta, \Theta^*\}$ .

Notably, both the choice of prior mean function and the treatment of hyperparameters influence the inferred results. The simplest strategy is to fix the GP hyperparameters and the parameters governing the mean function (e.g.,  $H_0$ ,  $\Omega_m$  in case of a  $\Lambda$ CDM prior mean) to their best-fit values. This method may yield tighter constraints with smaller error bars, as it conditions the reconstruction on a single point in parameter space. However, it does not fully capture the underlying model uncertainty, since it ignores the posterior spread in both the kernel and mean function parameters. In our implementation, we account for the full posterior over both kernel and mean function parameters, resulting in more realistic reconstructions.

# 5. ANALYSIS AND INTERPRETATION OF RESULTS

# 5.1. Kernel vs Cosmology: A Comparative Study

To assess the robustness of standard GP reconstruction and its sensitivity to the choice of kernel, we examine how different covariance functions affect the inferred value of the Hubble constant  $H_0$ . Table 1 presents the results obtained using various kernel types, which are described in Section 2.2.1.

Our findings indicate that the choice of kernel impacts both the central value and uncertainty of  $H_0$ . The inferred mean values span from 67.18 to 69.35 km/s/Mpc, although they are all compatible within  $1\sigma$ . The Matérn kernels show a systematic trend: increasing the smoothness parameter  $\nu$  (i.e., using smoother kernels) systematically lowers the predicted  $H_0$  and reduces its associated uncertainty. For instance, the relative error decreases from 9.13% for Matérn 3/2 to 7.23% for Matérn 9/2.

The SE kernel predicts the lowest  $H_0$  value (67.18 km/s/Mpc) with the smallest relative uncertainty (6.97 %), reflecting its highly smooth nature. Despite introducing additional hyperparameters to capture multi-scale correlations, the DSE kernel yields results comparable to the lower-order Matérn kernels with higher uncertainties. The reduced chi-squared values remain consistently below 0.5, indicating acceptable fits despite variations in the smoothness assumptions.

When comparing different cosmological models (as shown in Table 2), we observe similar trends. The  $\Lambda$ CDM model provides the most precise  $H_0$  estimate (68.84 km/s/Mpc) with a relative uncertainty of 4.11%. More flexible models, such as CPL, which introduce additional parameters, result in higher  $H_0$  values, but with correspondingly larger uncertainties. We also tested the Padé(2,2) parametrization C. Gruber & O. Luongo (2014), but found it poorly constrained by CC data alone due to parameter degeneracies. This is consistent with previous findings that Padé approximations require multi-probe datasets for stable constraints S. Capozziello et al. (2019).

In summary, both the choice of kernel and the cosmological model in the GP framework significantly influence the inferred value of the Hubble constant and its precision. Smoother kernels generally produce tighter constraints, while increased model complexity tends to widen uncertainties despite potential shifts in central values.

# 5.2. Hyperparameter Treatment: Optimization vs Marginalization

We compare two GP reconstruction strategies: utilizing the optimized hyperparameters (best-fit values) versus incorporating the full marginalized posteriors within the prediction function. In Figures 1 and 2, the shaded regions

| Parameter                    | Priors                   | Description  |  |
|------------------------------|--------------------------|--|--|
|                              | Kernel Hyperparameters   |  |  |
| $\log_{10}(\sigma_f)$        | $\mathcal{U}[-5,5]$      | overall amplitude of the correlation                                 |  |
| $\log_{10}(l_f)$             | $\mathcal{U}[-5,5]$      | coherence length of correlation                                      |  |
| $\log_{10}(\nu)$             | $\mathcal{U}[-2,1]$      | defines the smoothness of the kernel                                 |  |
|                              | Mean Function Parameters |  |  |
| $H_{0,\mathrm{hyper}}$       | $\mathcal{U}[50, 90]$    | Representative present expansion parameter in the mean function      |  |
| $\Omega_{m0,\mathrm{hyper}}$ | $\mathcal{U}[0.1, 0.5]$  | Representative present matter density parameter in the mean function |  |

**Table 3.** List of hyperparameters used in the training Gen GP and their corresponding priors. Uniform priors are chosen for all hyperparameters.

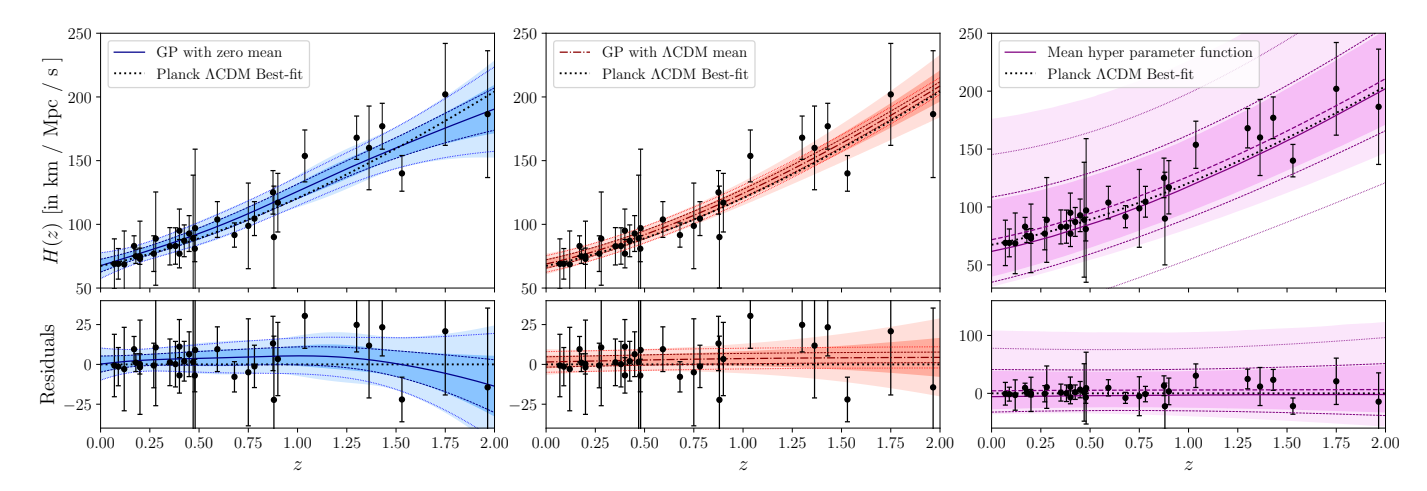


Figure 1. Reconstructed evolution of the Hubble parameter H(z) using GP with a Matérn  $\nu=3/2$  kernel (top panel). The black dotted curve denotes the *Planck* best-fit  $\Lambda$ CDM model. The blue and red shaded regions indicate the  $2\sigma$  confidence intervals obtained using a zero-mean prior function and a  $\Lambda$ CDM mean prior function, respectively, using the full marginalized posteriors, while the dashed and dotted lines show the  $1\sigma$  and  $2\sigma$  confidence intervals when optimized hyperparameters are employed. The distribution of the mean function for the corresponding hyperparameters is shown in magenta. Bottom panel shows residuals with respect to the *Planck*  $\Lambda$ CDM best-fit model. See Secs. 5.2 and 5.3 for details.

| Parameter                | $\sigma_f$                      | $l_f$                      | $ u_f$                    | $H_{0,\mathrm{hyper}}$       | $\Omega_{m0,\mathrm{hyper}}$ |
|--------------------------|---------------------------------|----------------------------|---------------------------|------------------------------|------------------------------|
| Zero mean                | $225.412_{-117.234}^{+543.440}$ | $5.550^{+16.454}_{-3.427}$ | $2.864^{+3.825}_{-1.640}$ | -                            | -                            |
| $\Lambda {\rm CDM}$ mean | $33.26^{+91.93}_{-25.63}$       | $6.01^{+2.760}_{-3.070}$   | $3.96^{+2.043}_{-2.141}$  | $68.218^{+14.056}_{-14.485}$ | $0.310^{+0.110}_{-0.099}$    |

Table 4. Constraints on hyperparameters with Gen GP when the a priori mean function is zero or  $\Lambda$ CDM. The Matérn Parameter  $\nu$  is free, and the constraints error bars quoted are at  $1\sigma$  confidence interval. See Sec. 5.4.

depict reconstructions using the full marginalized posteriors, while the dashed and dotted lines show the  $1\sigma$  and  $2\sigma$  confidence intervals when optimized hyperparameters are employed.

The leftmost panels of both figures reveal that there is no appreciable difference between these two reconstruction approaches, when employing a zero mean function<sup>15</sup>. This demonstrates that for zero-mean implementations, utilising best-fit hyperparameter values yields reconstructions equivalent in quality to those obtained from full posterior chains. This equivalence holds for both standard GP and Gen GP approaches with zero mean functions.

In contrast, the middle panel, which employs the  $\Lambda$ CDM mean function, reveals a notable divergence between the two reconstruction outcomes. The predicted H(z) values obtained from marginalised posteriors differ significantly from

<sup>&</sup>lt;sup>15</sup> This is consistent with previous findings in A. Favale et al. (2023), where the reconstructed shape of H(z) obtained with standard GP has been found to differ by 5% at most between marginalization and optimization procedure.

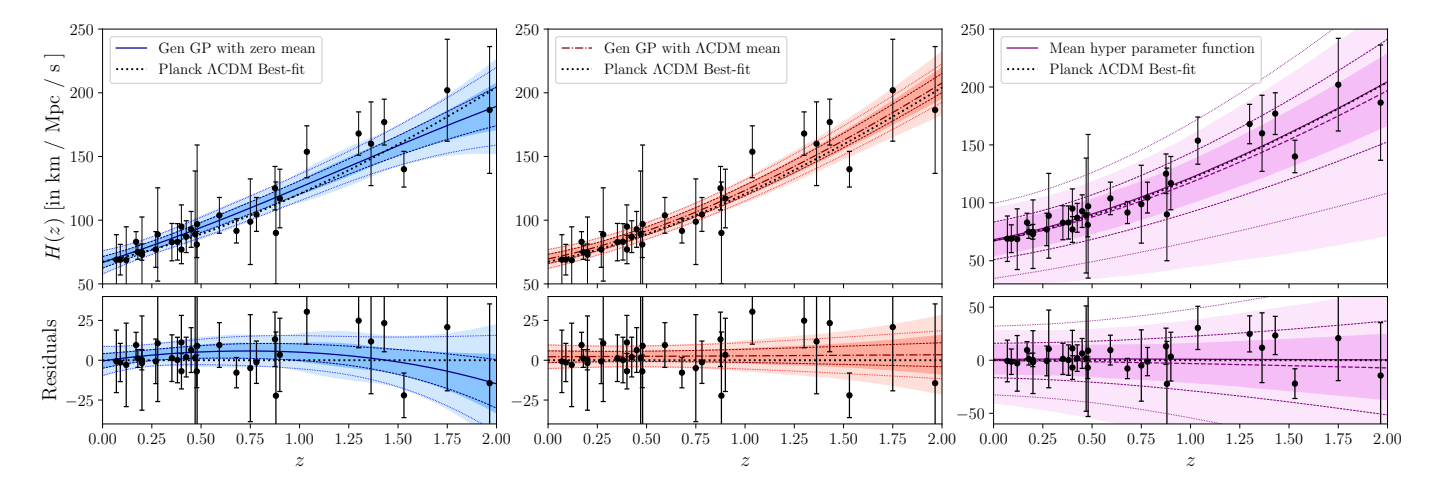


Figure 2. Reconstructed evolution of the Hubble parameter H(z) using Gen GP (top panel). The black dotted curve denotes the Planck best-fit  $\Lambda$ CDM model. The blue and red shaded regions indicate the  $2\sigma$  confidence intervals obtained using a zero-mean prior function and a  $\Lambda$ CDM mean prior function, respectively, using the full marginalized posteriors, while the dashed and dotted lines show the  $1\sigma$  and  $2\sigma$  confidence intervals when optimized hyperparameters are employed. The distribution of the mean function for the corresponding hyperparameters is also shown in magenta. Bottom panel shows residuals with respect to the Planck  $\Lambda$ CDM best-fit model. See Secs. 5.2 and 5.3 for details.

those derived using the optimised framework, particularly at redshifts z > 1. This discrepancy suggests that the choice of reconstruction method and the treatment of hyperparameters becomes crucial when incorporating cosmological priors through the mean function.

A particularly striking observation is that this reconstruction discrepancy is substantially reduced in the generalised GP compared to the standard GP implementation. The standard GP exhibits considerably larger discrepancies between the two methods, while Gen GP demonstrates much better agreement between marginalised and optimised approaches.

This enhanced consistency highlights Gen GP as the preferred choice for cosmological reconstructions when utilising the  $\Lambda$ CDM mean function, as it provides more robust results that are less sensitive to the specific implementation of hyperparameter treatment.

| Parameter | $H_{0,\mathrm{hyper}}$       | $H_0$ (zero mean function) | $H_0(\Lambda { m CDM mean function})$ |
|-----------|------------------------------|----------------------------|---------------------------------------|
| GP        | $61.647^{+44.294}_{-21.774}$ | $68.306^{+5.180}_{-5.177}$ | $68.914^{+4.064}_{-4.002}$            |
| Gen GP    | $68.218^{+14.056}_{-14.485}$ | $68.101^{+4.975}_{-4.909}$ | $69.563^{+4.150}_{-4.093}$            |

**Table 5.** Constraints on hyperparameter  $H_{0, \, \text{hyper}}$  when the a priori mean function  $\Lambda\text{CDM}$ , vs predicted cosmological  $H_0$  within Gen GP framework for both zero mean vs  $\Lambda\text{CDM}$  mean function scenarios. The Matérn kernel order parameter  $\nu$  is free, and the constraints error bars quoted are at  $1\sigma$  confidence interval. All values in km/s/Mpc. See Sec. 5.5.

# 5.3. Dissecting $\mu^*$ : Role of the GP mean function

The rightmost panels in Figures 1 and 2 provides crucial insight into the impact of the mean function  $\mu^*$  in cosmological reconstruction. There, we plot H(z) using only the mean function component,

$$H(z)_{\mu^*} = H_{0, \text{ hyper}} \left[ \Omega_{m0, \text{ hyper}} (1+z)^3 + (1 - \Omega_{m0, \text{ hyper}}) \right]^{\frac{1}{2}}.$$
 (18)

This expression corresponds to  $\mu^*$  in Equation (16) and represents the cosmological prior embedded within the full H(z) reconstruction shown in the middle panels. By isolating this component, we can examine how the hyperparameter  $H_0$  hyper differs from the cosmologically inferred  $H_0$ .

 $H_{0, \text{hyper}}$  differs from the cosmologically inferred  $H_0$ . Our MCMC analysis yields  $H_{0, \text{hyper}} = 61.647^{+44.294}_{-21.774}$  km/s/Mpc for standard GP and  $H_{0, \text{hyper}} = 68.218^{+14.056}_{-14.485}$  km/s/Mpc for Gen GP. These large uncertainties reflect the broad prior range and inherent flexibility built into the hyperparameter framework. However, the final reconstructed Hubble function exhibits significantly tighter constraints,

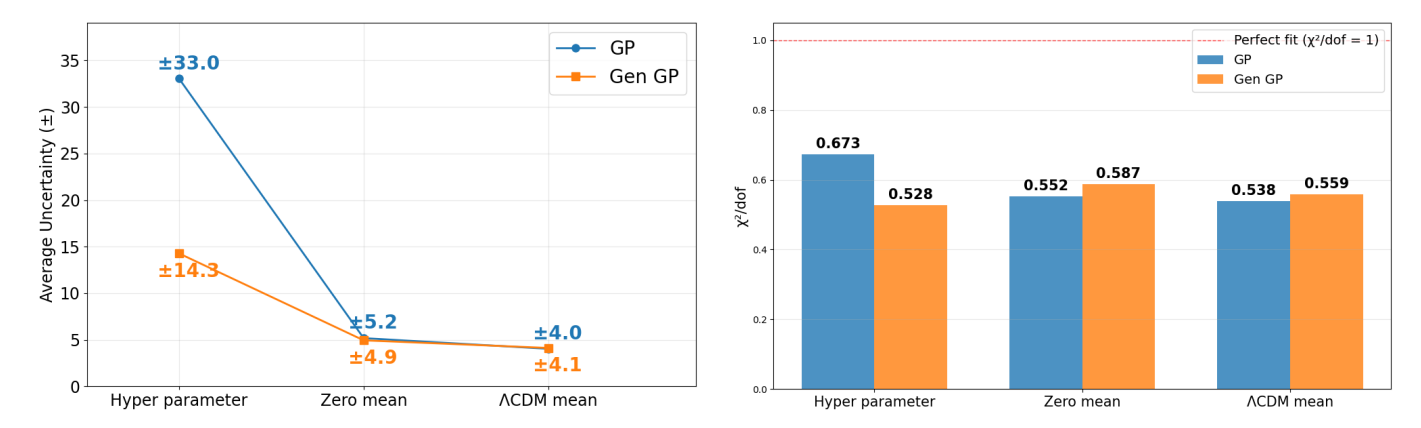


Figure 3. The left panel shows the variation of uncertainty in the Hubble constant parameter for both GP and GenGP reconstructions, using both zero mean and  $\Lambda$ CDM mean functions. For comparison, we also include the case where only the mean function (assumed as  $\Lambda$ CDM) is used, without the full GP or GenGP modeling, prior to applying the covariance matrix (Eq. 18). The right panel presents a comparison of the corresponding  $\chi^2$  values for each case.

with uncertainties of approximately  $\pm 5$  km/s/Mpc at z=0, as evident in the leftmost and middle panels of both figures. Similar findings are summarised in Table 5.

This apparent contradiction stems from the fundamental distinction between the hyperparameter  $H_{0, \text{hyper}}$  and the actual reconstructed H(z) at z=0. The hyperparameter serves as a regularisation framework that enables the Gaussian process to capture the general functional form of cosmological expansion, while the final reconstruction represents a data-driven synthesis incorporating information from the mean function, kernel correlations, and observational constraints.

Our analysis employs both maximum a posteriori (MAP) estimates of hyperparameters and marginalisation over their full posterior distributions. Notably, we demonstrate that when utilising the  $\Lambda$ CDM mean function, the full marginalization approach provides enhanced reconstruction performance compared to MAP treatment, particularly in terms of consistency between different GP implementations.

# 5.4. Interpreting GP Hyperparameters vs Physical Cosmological Parameters

The GP frameworks employed in our analysis includes hyperparameters  $H_{0, \text{hyper}}$  and  $\Omega_{m0, \text{hyper}}$  within the mean function. While these two representative parameters are cosmologically motivated, they serve a fundamentally different role than their physical counterparts in cosmological models.

In traditional cosmological analysis,  $H_0$  refers to the Hubble constant, physically interpreted as the current expansion rate of the Universe and typically constrained to values around 67-73 km/s/Mpc, depending on the dataset and methodology employed L. Verde et al. (2024). Similarly,  $\Omega_{m0}$  denotes the present-day matter density parameter, representing the fraction of the critical density contributed by matter, with observational constraints typically placing it around 0.3 N. Aghanim et al. (2020).

In contrast, the hyperparameters  $H_{0, \text{hyper}}$  and  $\Omega_{m0, \text{hyper}}$  in our GP mean function act as flexible reference/representative parameters that allow the model to capture the general functional form of cosmological expansion without being rigidly tied to specific physical values. These hyperparameters provide GP with a cosmologically-motivated priors, enabling it to model the Hubble parameter-redshift relationships that approximately follow familiar cosmological behavior while retaining the flexibility to deviate from standard cosmological predictions where the data warrants it.

The broad uniform priors assigned to these hyperparameters  $(H_{0, \text{hyper}} \in \mathcal{U}[50, 90])$  in km/s/Mpc and  $\Omega_{m0, \text{hyper}} \in \mathcal{U}[0.1, 0.5]$ ) reflect this distinction. Rather than representing precise physical constraints, these ranges allow the GP to explore a wide parameter space and let the data determine the optimal baseline behavior. This approach enables model-independent reconstruction of the expansion history while maintaining computational stability through a physically reasonable mean function structure.

Accordingly, the wide and weakly constrained results for  $H_{0,\text{hyper}}$  and  $\Omega_{m,\text{hyper}}$  shown in Table 4 are expected. These hyperparameters do not carry direct physical significance within the GP framework but can offer insight into interpreting of cosmological behavior that the reconstructed expansion history most closely resembles.

# 5.5. Quantitative comparison: GP vs Gen GP

The transition from standard GP to Gen GP yields substantial improvements in reconstruction quality and consistency. Table 5 provides a comprehensive comparison of the  $H_0$  constraints obtained under different mean function assumptions for both methodologies.

For hyperparameter constraints, Gen GP demonstrates significantly tighter bounds on  $H_{0, \text{hyper}}$  compared to standard GP. The hyperparameter uncertainty reduces from  $H_0 = 61.647^{+44.294}_{-21.774} \text{ km/s/Mpc}$  in standard GP to  $H_0 = 68.218^{+14.056}_{-14.485} \text{ km/s/Mpc}$  in Gen GP, representing approximately a 60% reduction in uncertainty while maintaining consistent central values.

When employing zero mean functions, both approaches yield comparable results:  $H_0 = 68.306^{+5.180}_{-5.177}$  km/s/Mpc for GP and  $H_0 = 68.101^{+4.975}_{-4.909}$  km/s/Mpc for Gen GP. The marginal improvement in Gen GP reflects the enhanced flexibility from the additional free parameter  $\nu$ . The corresponding reduced chi-squared statistics are  $\chi^2/\text{dof} = 0.552$  for standard GP and  $\chi^2/\text{dof} = 0.587$  for Gen GP, with Gen GP showing slightly higher values due to its increased model flexibility<sup>16</sup>. We note that although the  $\chi^2/\text{dof}$  values do not approach unity, the derived uncertainties are highly consistent with the scatter observed in the best-fit values of  $H_0$ . This behavior likely reflects our choice of dataset, as similar  $\chi^2/\text{dof}$  values are obtained for cosmological models (see Table 2). As discussed in Section 3.1, these statistics will improve as additional observational datasets are incorporated. Currently, we consider the model with  $\chi^2/\text{dof}$  closest to unity as providing the best fit.

The most significant improvements emerge when utilising  $\Lambda$ CDM mean functions. Gen GP yields  $H_0 = 69.563^{+4.150}_{-4.093}$  km/s/Mpc, demonstrating slightly larger central values but comparable uncertainties to standard GP viz.  $H_0 = 68.914^{+4.064}_{-4.002}$  km/s/Mpc. The reduced chi-squared values are  $\chi^2/\text{dof} = 0.538$  for standard GP and  $\chi^2/\text{dof} = 0.559$  for Gen GP. However, the crucial difference lies in the reconstruction consistency discussed in Section 5.2.

A key advantage of Gen GP becomes evident when comparing reconstruction methodologies. In Gen GP, the difference between using optimised hyperparameters (best-fit) and full marginalised posteriors in the prediction function is significantly smaller compared to standard GP (Figures 1 and 2, middle panels). This enhanced consistency highlights Gen GP as a better candidate for reconstruction, especially when employing the  $\Lambda$ CDM mean function, due to its improved stability at higher redshifts (z > 1) where standard GP exhibits substantial methodological dependence.

The modest increase in chi-squared values for Gen GP across both mean function implementations reflects the additional flexibility introduced by allowing  $\nu$  to vary freely. This trade-off between slightly higher chi-squared and enhanced model adaptability represents a beneficial exchange, as Gen GP provides more realistic uncertainty estimates while maintaining fair agreement with observational data. The ability to tune kernel smoothness directly from data, rather than fixing it a priori, makes Gen GP particularly valuable for robust cosmological inference.

These comprehensive results demonstrate that Gen GP outperforms standard GP implementations where either cosmological assumptions are rigidly imposed or Matérn kernel parameters are fixed to predetermined values. The enhanced flexibility, improved reconstruction consistency, and more realistic uncertainty quantification establish Gen GP as the preferred competitive framework for model-independent cosmological analysis.

To summarize, Gen GP demonstrates better performance through several key advantages:

- 1. significantly reduced discrepancy between optimized and marginalized reconstruction approaches, especially for  $\Lambda$ CDM mean function;
- 2. improved chi-squared statistics;
- 3. stable uncertainty bands.

When  $\nu$  is kept free within the prior uniform range  $\nu \in \mathcal{U}[0.5, 7]$ , Gen GP yields  $H_0 = 69.563^{+4.150}_{-4.093}$  km/s/Mpc, representing a fully generalised approach that avoids over-smoothing associated with fixed kernel choices while maintaining consistency across different redshift ranges.

<sup>&</sup>lt;sup>16</sup> Table 1 uses optimized hyperparameters, Section 5.3 uses marginalized hyperparameters.

## 6. CONCLUSIONS

This work systematically investigates uncertainties in inference of Hubble constant,  $H_0$ , arising from Gaussian Process reconstruction, introducing the Generalised Gaussian Process (Gen GP) framework to address fundamental limitations in current GP implementations.

Our analysis reveals that kernel selection introduces systematic variations in  $H_0$  estimates comparable to those caused by different cosmological models. Across six different kernels, namely Matérn  $\nu = 3/2, 5/2, 7/2, 9/2$ , as well as SE and DSE, the inferred  $H_0$  values range from 67.18 to 69.35 km/s/Mpc, similar to the spread observed between  $\Lambda$ CDM ( $H_0 = 68.84 \pm 4.11$  km/s/Mpc) and dynamical DE models like CPL ( $H_0 = 70.97 \pm 6.74$  km/s/Mpc). The Gen GP framework mitigates this kernel selection bias by treating the Matérn order (smoothness) parameter  $\nu$  as a free parameter, allowing data to determine optimal kernel structure.

A key finding relates to reconstruction methodology. Gen GP demonstrates significantly enhanced consistency between reconstructions undertaken with optimized hyperparameter and full marginalisation approaches, compared to traditional GP, especially when the  $\Lambda$ CDM mean function is employed. Within this context, traditional GP exhibits substantial differences between best-fit and marginalised reconstruction frameworks, particularly at higher redshifts (z>1), while Gen GP maintains remarkable stability across both methodologies. This consistency, combined with only modest increases in chi-squared values ( $\chi^2/\text{dof}=0.587$  vs 0.552 for zero mean; 0.559 vs 0.538 for  $\Lambda$ CDM mean), reflects beneficial flexibility gains that provide more realistic uncertainty band estimates without compromising with the data quality.

Our results highlight three key requirements for reliable, model-independent cosmological inference:

- treating kernel parameters as free to avoid selection bias;
- full Bayesian marginalization over hyperparameters to properly capture model uncertainties;
- accepting broader uncertainty bands as honest reflections of methodological limitations.

As ML is expected to play an increasingly central role in upcoming surveys – such as Euclid and LSST – maintaining methodological rigor becomes even more crtitcal. The Gen GP framework offers a robust, flexible, and principled approach to cosmological inference that captures essential uncertainties while remaining agnostic to specific model assumptions.

# ACKNOWLEDGEMENTS

The authors would like to thank J.E. González for his valuable collaboration and insightful suggestions during the initial phase of this work. We would also like to thank Anto I. Ionnappan and Anjan Ananda Sen for their valuable suggestions and comments on the manuscript. We acknowledge Giacomo Gradenigo for helpful discussions.

Ruchika is supported by "Theoretical Astroparticle Physics" (TAsP), an iniziativa specifica INFN, and by Project SA097P24 funded by Junta de Castilla y León. PM acknowledges funding from the Anusandhan National Research Foundation (ANRF), Govt of India, under the National Post-Doctoral Fellowship (File no. PDF/2023/001986).

We acknowledge the use of the HPC facility, Pegasus, at IUCAA, Pune, India. This article/publication is based upon work from COST Action CA21136- "Addressing observational tensions in cosmology with systematics and fundamental physics (CosmoVerse)", supported by COST (European Cooperation in Science and Technology).

# REFERENCES

Abbott, T. M. C., et al. 2022, Phys. Rev. D, 105, 023520, doi: 10.1103/PhysRevD.105.023520

Abramowitz, M., & Stegun, I. A. 1964, Handbook of Mathematical Functions (Dover Publications)

Adachi, M., & Kasai, M. 2012, Progress of Theoretical Physics, 127, 145

Ade, P. A. R., et al. 2016, Astron. Astrophys., 594, A13, doi: 10.1051/0004-6361/201525830 Aghanim, N., et al. 2020, Astron. Astrophys., 641, A6, doi: 10.1051/0004-6361/201833910

Aviles, A., Bravetti, A., Capozziello, S., & Luongo, O. 2014, Phys. Rev. D, 90, 043531, doi: 10.1103/PhysRevD.90.043531

Ball, N. M., & Brunner, R. J. 2010, International Journal of Modern Physics D, 19, 1049

Banerjee, N., Mukherjee, P., & Pavón, D. 2023, JCAP, 11, 092, doi: 10.1088/1475-7516/2023/11/092

- Baron, D. 2019, arXiv preprint arXiv:1904.07248
- Berger, P., & Stein, G. 2019, Mon. Not. Roy. Astron. Soc., 482, 2861, doi: 10.1093/mnras/sty2949
- Bishop, C. M. 2006, Pattern Recognition and Machine Learning (New York: Springer)
- Blanchard, A., et al. 2020, Astron. Astrophys., 642, A191, doi: 10.1051/0004-6361/202038071
- Busti, V. C., Clarkson, C., & Seikel, M. 2014, Mon. Not. Roy. Astron. Soc., 441, 11, doi: 10.1093/mnrasl/slu035
- Caldeira, J., Wu, W. L. K., Nord, B., et al. 2019, Astron. Comput., 28, 100307, doi: 10.1016/j.ascom.2019.100307
- Capozziello, S., Ruchika, & Sen, A. A. 2019, Mon. Not. Roy. Astron. Soc., 484, 4484, doi: 10.1093/mnras/stz176
- Charnock, T., Lavaux, G., & Wandelt, B. D. 2018, Phys. Rev. D, 97, 083004, doi: 10.1103/PhysRevD.97.083004
- Charnock, T., Lavaux, G., Wandelt, B. D., et al. 2020, MNRAS, 494, 50, doi: 10.1093/mnras/staa682
- Chevallier, M., & Polarski, D. 2001, Int. J. Mod. Phys. D, 10, 213, doi: 10.1142/S0218271801000822
- Cortes, C., & Vapnik, V. 1995, Machine Learning, 20, 273, doi: 10.1007/BF00994018
- Di Valentino, E., Anchordoqui, L. A., Akarsu, Ö., et al. 2021, Astroparticle Physics, 131, 102605
- Dutta, K., Ruchika, Roy, A., Sen, A. A., & Sheikh-Jabbari, M. M. 2020, Gen. Rel. Grav., 52, 15, doi: 10.1007/s10714-020-2665-4
- Dvorkin, C., et al. 2022, in Snowmass 2021. https://arxiv.org/abs/2203.08056
- Evslin, J., Sen, A. A., & Ruchika. 2018, Phys. Rev. D, 97, 103511, doi: 10.1103/PhysRevD.97.103511
- Favale, A., Dainotti, M. G., Gómez-Valent, A., & Migliaccio, M. 2024, JHEAp, 44, 323, doi: 10.1016/j.jheap.2024.10.010
- Favale, A., Gómez-Valent, A., & Migliaccio, M. 2023, Mon. Not. Roy. Astron. Soc., 523, 3406, doi: 10.1093/mnras/stad1621
- Forconi, M., Giarè, W., Mena, O., et al. 2024, JCAP, 05, 097, doi: 10.1088/1475-7516/2024/05/097
- Forconi, M., Ruchika, Melchiorri, A., Mena, O., & Menci, N. 2023, JCAP, 10, 012,
  - doi: 10.1088/1475-7516/2023/10/012
- Foreman-Mackey, D., Hogg, D. W., Lang, D., & Goodman, J. 2013, Publications of the Astronomical Society of the Pacific, 125, 306, doi: 10.1086/670067
- Friedman, J. H. 2001, The Annals of Statistics, 29, 1189, doi: 10.1214/aos/1013203451
- Géron, A. 2019, Hands-On Machine Learning with Scikit-Learn, Keras, and TensorFlow, 2nd edn. (Sebastopol, CA: O'Reilly Media)

- Geurts, P., Ernst, D., & Wehenkel, L. 2006, Machine Learning, 63, 3, doi: 10.1007/s10994-006-6226-1
- Gómez-Valent, A. 2022, Phys. Rev. D, 105, 043528, doi: 10.1103/PhysRevD.105.043528
- Gómez-Valent, A., & Amendola, L. 2018, JCAP, 04, 051, doi: 10.1088/1475-7516/2018/04/051
- Goodfellow, I., Bengio, Y., & Courville, A. 2016, Deep Learning (MIT Press).
  - http://www.deeplearningbook.org
- Gruber, C., & Luongo, O. 2014, Phys. Rev. D, 89, 103506, doi: 10.1103/PhysRevD.89.103506
- Handley, W. 2019, Journal of Cosmology and Astroparticle Physics, 2019, 054, doi: 10.1088/1475-7516/2019/03/054
- Haridasu, B. S., Luković, V. V., Moresco, M., & Vittorio, N. 2018, JCAP, 10, 015,
  - doi: 10.1088/1475-7516/2018/10/015
- Harnois-Dérap s, J., Giblin, B., & Joachimi, B. 2019, Astronomy & Astrophysics, 631, A160, doi: 10.1051/0004-6361/201935912
- Harris, C. R., Millman, K. J., Van Der Walt, S. J., et al. 2020, nature, 585, 357
- Hassan, S., Liu, A., Kohn, S., & Plante, P. L. 2019, Monthly Notices of the Royal Astronomical Society, 483, 2524, doi: 10.1093/mnras/sty3282
- Heymans, C., et al. 2021, Astron. Astrophys., 646, A140, doi: 10.1051/0004-6361/202039063
- Holland, J. H. 1992, Adaptation in Natural and Artificial Systems, revised edition edn. (MIT Press)
- Holsclaw, T., Alam, U., Sansó, B., et al. 2010, Phys. Rev. Lett., 105, 241302, doi: 10.1103/PhysRevLett.105.241302
- Holsclaw, T., Alam, U., Sansó, B., et al. 2011, Physical Review D-Particles, Fields, Gravitation, and Cosmology, 84, 083501
- Hunter, J. D. 2007, Computing in Science & Engineering, 9, 90, doi: 10.1109/MCSE.2007.55
- Hwang, S.-g., L'Huillier, B., Keeley, R. E., Jee, M. J., & Shafieloo, A. 2023, JCAP, 02, 014, doi: 10.1088/1475-7516/2023/02/014
- Ivezić, Ž., et al. 2019, Astrophys. J., 873, 111, doi: 10.3847/1538-4357/ab042c
- Jeffrey, N., Lanusse, F., Lahav, O., & Starck, J.-L. 2020, Mon. Not. Roy. Astron. Soc., 492, 5023, doi: 10.1093/mnras/staa127
- Jiang, J.-y., Jiao, K., & Zhang, T.-J. 2025, https://arxiv.org/abs/2506.21238
- Jimenez, R., & Loeb, A. 2002, Astrophys. J., 573, 37, doi: 10.1086/340549
- Johnson, J. P., & Jassal, H. K. 2025, Eur. Phys. J. C, 85, 996, doi: 10.1140/epjc/s10052-025-14732-7

- Knox, L., & Millea, M. 2020, Phys. Rev. D, 101, 043533, doi: 10.1103/PhysRevD.101.043533
- Krishnan, C., Colgáin, E. Ó., Ruchika, et al. 2020, Phys.Rev. D, 102, 103525, doi: 10.1103/PhysRevD.102.103525
- LeCun, Y., Bengio, Y., & Hinton, G. 2015, Nature, 521, 436, doi: 10.1038/nature14539
- Lemos, T., Ruchika, Carvalho, J. C., & Alcaniz, J. 2023, Eur. Phys. J. C, 83, 495, doi: 10.1140/epjc/s10052-023-11651-3
- Lewis, A. 2019, https://arxiv.org/abs/1910.13970
- Li, Z., Zhang, B., & Liang, N. 2023, Monthly Notices of the Royal Astronomical Society, 521, 4406, doi: 10.1093/mnras/stad838
- Liang, N., Li, Z., Xie, X., & Wu, P. 2022, Astrophys. J., 941, 84, doi: 10.3847/1538-4357/aca08a
- Linder, E. V. 2003, Phys. Rev. Lett., 90, 091301, doi: 10.1103/PhysRevLett.90.091301
- Lochner, M., McEwen, J. D., Peiris, H. V., Lahav, O., & Winter, M. K. 2016, Astrophys. J. Suppl., 225, 31, doi: 10.3847/0067-0049/225/2/31
- Lonappan, A. I., Kumar, S., Ruchika, Dinda, B. R., & Sen, A. A. 2018, Phys. Rev. D, 97, 043524, doi: 10.1103/PhysRevD.97.043524
- Lucie-Smith, L., Peiris, H. V., Pontzen, A., Nord, B., & Thiyagalingam, J. 2024, Phys. Rev. D, 109, 063524, doi: 10.1103/PhysRevD.109.063524
- MacKay, D. J. C. 2002, Information Theory, Inference & Learning Algorithms (Cambridge University Press)
  Mandelbaum, R., et al. 2018,

https://arxiv.org/abs/1809.01669

- Merten, J., Giocoli, C., Baldi, M., et al. 2019, MNRAS, 487, 104, doi: 10.1093/mnras/stz972
- Modi, C., Feng, Y., & Seljak, U. 2018, JCAP, 10, 028, doi: 10.1088/1475-7516/2018/10/028
- Moresco, M. 2024, arXiv preprint 2412.01994. https://arxiv.org/abs/2412.01994
- Moresco, M., et al. 2022, Living Rev. Rel., 25, 6, doi: 10.1007/s41114-022-00040-z
- Mukherjee, P., & Banerjee, N. 2021, Eur. Phys. J. C, 81, 36, doi: 10.1140/epjc/s10052-021-08830-5
- Mukherjee, P., Dainotti, M. G., Dialektopoulos, K. F., Levi Said, J., & Mifsud, J. 2026, JHEAp, 49, 100439, doi: 10.1016/j.jheap.2025.100439
- Mukherjee, P., Dey, A., & Pal, S. 2024a, https://arxiv.org/abs/2407.19481
- Mukherjee, P., Dialektopoulos, K. F., Levi Said, J., & Mifsud, J. 2024b, JCAP, 09, 060, doi: 10.1088/1475-7516/2024/09/060

- Mukherjee, P., & Sen, A. A. 2024, Phys. Rev. D, 110, 123502, doi: 10.1103/PhysRevD.110.123502
- Mukherjee, P., & Sen, A. A. 2025, https://arxiv.org/abs/2505.19083
- Münchmeyer, M., & Smith, K. M. 2019, https://arxiv.org/abs/1905.05846
- Murphy, K. P. 2012, Machine Learning: A Probabilistic Perspective (Cambridge, MA: MIT Press)
- Neal, R. M. 1996, Bayesian Learning for Neural Networks (Springer-Verlag)
- Ntampaka, M., Trac, H., Sutherland, D. J., et al. 2015,
  Astrophys. J., 803, 50, doi: 10.1088/0004-637X/803/2/50
  Ntampaka, M., et al. 2019,

https://arxiv.org/abs/1902.10159

- Padmanabhan, T. 2003, Phys. Rept., 380, 235, doi: 10.1016/S0370-1573(03)00120-0
- Patil, T., Ruchika, & Panda, S. 2024, JCAP, 05, 033, doi: 10.1088/1475-7516/2024/05/033
- Price-Whelan, A. M., Sipőcz, B., Günther, H., et al. 2018, The Astronomical Journal, 156, 123
- Price-Whelan, A. M., Lim, P. L., Earl, N., et al. 2022, The Astrophysical Journal, 935, 167
- Rasmussen, C. E., & Nickisch, H. 2010, Journal of Machine Learning Research, 11, 3011.

http://jmlr.org/papers/v11/rasmussen10a.html

- Rasmussen, C. E., & Williams, C. K. I. 2006, Gaussian Processes for Machine Learning (MIT Press)
- Ravanbakhsh, S., Lanusse, F., Mandelbaum, R., Schneider, J., & Poczos, B. 2016, https://arxiv.org/abs/1609.05796
- Raveri, M., & Hu, W. 2019, Phys. Rev. D, 99, 043506, doi: 10.1103/PhysRevD.99.043506
- Ribli, D., Pataki, B. Á., Zorrilla Matilla, J. M., et al. 2019, Mon. Not. Roy. Astron. Soc., 490, 1843, doi: 10.1093/mnras/stz2610
- Riess, A. G., et al. 2022, Astrophys. J. Lett., 934, L7, doi: 10.3847/2041-8213/ac5c5b
- Robitaille, T. P., Tollerud, E. J., Greenfield, P., et al. 2013, Astronomy & Astrophysics, 558, A33
- Ruchika, Adil, S. A., Dutta, K., Mukherjee, A., & Sen, A. A. 2023, Phys. Dark Univ., 40, 101199, doi: 10.1016/j.dark.2023.101199
- Ruchika, Giarè, W., Teixeira, E. M., & Melchiorri, A. 2025, Phys. Dark Univ., 49, 101999, doi: 10.1016/j.dark.2025.101999
- Schmelzle, J., Lucchi, A., Kacprzak, T., et al. 2017, arXiv preprint arXiv:1707.05167
- Seikel, M., Clarkson, C., & Smith, M. 2012, JCAP, 06, 036, doi: 10.1088/1475-7516/2012/06/036
- Sellentin, E., & Heavens, A. F. 2016, Mon. Not. Roy. Astron. Soc., 456, L132, doi: 10.1093/mnrasl/slv190

- Shafieloo, A., Kim, A. G., & Linder, E. V. 2012, Physical Review D—Particles, Fields, Gravitation, and Cosmology, 85, 123530
- Smith, T. L., Poulin, V., Bernal, J. L., et al. 2021, Phys. Rev. D, 103, 123542, doi: 10.1103/PhysRevD.103.123542
- Sun, W., Jiao, K., & Zhang, T.-J. 2021, Astrophys. J., 915, 123, doi: 10.3847/1538-4357/ac05b8
- Velázquez, J. d. J., Escamilla, L. A., Mukherjee, P., & Vázquez, J. A. 2024, Universe, 10, 464, doi: 10.3390/universe10120464
- Verde, L. 2010, in Lectures on Cosmology: Accelerated Expansion of the Universe (Springer), 147–177
- Verde, L., Schöneberg, N., & Gil-Marín, H. 2024, Ann. Rev. Astron. Astrophys., 62, 287,
  - doi: 10.1146/annurev-astro-052622-033813
- Verde, L., Treu, T., & Riess, A. G. 2019, Nature Astronomy, 3, 891, doi: 10.1038/s41550-019-0902-0
- Villaescusa-Navarro, F., et al. 2020, Astrophys. J. Suppl., 250, 2, doi: 10.3847/1538-4365/ab9d82

- Virtanen, P., Gommers, R., Oliphant, T. E., et al. 2020, Nature methods, 17, 261
- Wang, G.-J., Shi, H.-L., Yan, Y.-P., et al. 2022, Astrophys.
  J. Supp., 260, 13, doi: 10.3847/1538-4365/ac5f4a
- Weinberg, S. 1989, Rev. Mod. Phys., 61, 1, doi: 10.1103/RevModPhys.61.1
- Wilde, J., Serjeant, S., Bromley, J. M., et al. 2022, Monthly Notices of the Royal Astronomical Society, 512, 3464
- Yang, Y., & Gong, Y. 2021, Mon. Not. Roy. Astron. Soc., 504, 3092, doi: 10.1093/mnras/stab1085
- Yang, Y., Lu, X., Qian, L., & Cao, S. 2023, Mon. Not. Roy. Astron. Soc., 519, 4938, doi: 10.1093/mnras/stac3617
- Zorrilla Matilla, J. M., Sharma, M., Hsu, D., & Haiman, Z. 2020, Phys. Rev. D, 102, 123506, doi: 10.1103/PhysRevD.102.123506